Nuclear Engineering and Technology xxx (xxxx) xxx

Contents lists available at ScienceDirect

Nuclear Engineering and Technology

journal homepage: www.elsevier.com/locate/net

Numerical analysis on in-core ignition and subsequent flame propagation to containment in OPR1000 under loss of coolant accident

Chang Hyun Song [a], Joon Young Bae [a], Sung Joong Kim [a, b, *]

[a] Department of Nuclear Engineering, Hanyang University, 222 Wangsimni-ro, Seongdong-gu, Seoul 04763, Republic of Korea
[b] Institute of Nano Science & Technology, Hanyang University, 222 Wangsimni-ro, Seongdong-gu, Seoul 04763, Republic of Korea

ARTICLE INFO

Article history:
Received 14 November 2021
Received in revised form
6 February 2022
Accepted 19 March 2022

Keywords:
Severe accident
Hydrogen
Combustion
Flame propagation
MELCOR
SAMG

ABSTRACT

Since Fukushima nuclear power plant (NPP) accident in 2011, the importance of research on various severe accident phenomena has been emphasized. Particularly, detailed analysis of combustion risk is necessary following the containment damage caused by combustion in the Fukushima accident. Many studies have been conducted to evaluate the risk of local hydrogen concentration increases and flame propagation using computational code. In particular, the potential for combustion by local hydrogen concentration in specific areas within the containment has been emphasized. In this study, the process of flame propagation generated inside a reactor core to containment during a loss of coolant accident (LOCA) was analyzed using MELCOR 2.1 code. Later in the LOCA scenario, it was expected that hydrogen combustion occurred inside the reactor core owing to oxygen inflow through the cold leg break area. The main driving force of the oxygen intrusion is the elevated containment pressure due to the molten corium–concrete interaction. The thermal and mechanical loads caused by the flame threaten the integrity of the containment. Additionally, the containment spray system effectiveness in this situation was evaluated because changes in pressure gradient and concentrations of flammable gases greatly affect the overall behavior of ignition and subsequent containment integrity.

1. Introduction

Since the Fukushima nuclear power plant (NPP) accident occurred in 2011, the significance of safety analysis for various phenomena during severe accidents has been emphasized. In particular, it was confirmed that radioactive materials were released into the environment owing to the containment damage caused by the combustion of flammable gases. Accordingly, combustion risk analysis has been considered an important issue to guarantee the integrity of the containment, which is the last barrier for the prevention of radioactive material leakage. Flammable gases, such as hydrogen and carbon monoxide, can be concentrated in the local region because of the complex geometry of the NPP structure, such that concentrations can increase up to ignition criteria, which is concentration required to be ignited. A flame produced locally can propagate throughout the entire containment if the propagation criteria are satisfied, inflicting thermal and mechanical loads on all structures and walls. A drastic rise in temperature and pressure can threaten the integrity of the containment.

In severe accidents, flammable gases can be generated by various phenomena during both the in-vessel and ex-vessel phases. Hydrogen can be generated in the reactor core during core degradation. In a design basis accident (DBA) or beyond design basis accident (BDBA), when the decay heat is not sufficiently removed by the coolant, the core water level gradually decreases. The oxidation reaction with the generated steam starts from the upper cladding, which is composed of Zr [1]. As Zr is oxidized by steam, a large amount of hydrogen is generated. Furthermore, flammable gases are generated during molten corium–concrete interaction (MCCI) after reactor pressure vessel (RPV) failure. When the cavity concrete is decomposed, hydrogen and carbon monoxide are generated. In particular, a large amount of carbon monoxide is generated from the basaltic concrete of the optimized pressurized reactor 1000 (OPR1000) [2].

* Corresponding author. Department of Nuclear Engineering, Hanyang University, 222 Wangsimni-ro, Seongdong-gu, Seoul 04763, Republic of Korea.
E-mail address: sungjkim@hanyang.ac.kr (S.J. Kim).

https://doi.org/10.1016/j.net.2022.03.023

Abbreviations

APR1400	Advanced Power Reactor 1400
BDBA	Beyond Design Basis Accident
CAFT	Calculated Adiabatic Flame Temperature
CET	Core Exit Temperature
CFD	Computational Fluid Dynamics
CNAFT	Calculated Non-Adiabatic Flame Temperature
CNMT	Containment
CSS	Containment Spray System
CV	Control Volume
DBA	Design Basis Accident
ESF	Engineered Safety Feature
FSAR	Final Safety Analysis Report
IRWST	In-containment Refueling Water Storage Tank
LBLOCA	Large Break Loss of Coolant Accident
LFL	Lower Flammability Limit
LOFW	Loss of Feed Water
LOCA	Loss of Coolant Accident
LP	Lumped Parameter
MCCI	Molten Corium-Concrete Interaction
MS	Mitigation Strategy
NPP	Nuclear Power Plant
OPR1000	Optimized Pressurized Reactor 1000
PAR	Passive Automatic Recombiner
RCS	Reactor Coolant System
RPV	Reactor Pressure Vessel
SA	Severe Accident
SAMG	Severe Accident Management Guide
SBLOCA	Small Break Loss of Coolant Accident
SBO	Station Blackout
SG	Steam Generator
TLOFW	Total Loss of Feed Water
TSC	Technical Support Center
UFL	Upper Flammability Limit

Nomenclature

L	Flammability limit (volume fraction)
LFL	Lower flammability limit (volume fraction)
X	Gas concentration (volume fraction)

Constant generation of flammable gases during the overall accident phase means that the concentration can gradually increase as the accident progresses. This implies that the containment becomes more vulnerable to combustion. Furthermore, the vulnerability can become greater when the mitigation strategy is implemented. When the containment spray system (CSS) is activated by the operator to control the pressure of the containment, the concentration of flammable gases increases because the steam is condensed by the water droplets. Therefore, analyzing the combustibility of the gas mixture that can be formed in an NPP is necessary. In particular, evaluating the flammability by the concentration of hydrogen is important because hydrogen has the widest flammability range in air (4–75%) among the flammable gases generated in a NPP [3].

Hydrogen can be combusted by reacting with oxygen, given a sufficient concentration above a certain criterion for the generated flame to propagate. To propagate continuously, the concentration should be in the range between the upper flammability limit (UFL) and lower flammability limit (LFL). The UFL and LFL are the maximum and minimum concentrations required for propagation, respectively. It was found that the flammability limit of hydrogen varies depending on the composition ratio of steam–air in a gaseous mixture [4]. Based on this finding, many experimental studies have been conducted to evaluate the dependence of the composition and thermal properties on the flammability limits of various hydrogen mixtures [5–10]. Hustad et al. conducted an experimental study on the LFL of a hydrogen–methane–butane–carbon monoxide mixture [5]. The required hydrogen concentration decreased when other flammable gases were present or when the initial temperature was high. Based on this result, a new mixing rule was suggested, which predicts the LFL of the mixture at elevated temperatures, simplifying Le Chatelier's formula. Schoor et al. conducted an experiment to evaluate the pressure and temperature dependence of the UFL of methane–hydrogen–air mixtures [6]. The UFL increased when the initial temperature and pressure were higher, thus the flammability range increased. Through many experimental results, it was confirmed that the coexistence of flammable gases with hydrogen and higher initial temperature and pressure increased the combustion risk by lowering the LFL or raising the UFL. This indicates that the flammability range of hydrogen increases.

Based on experimental results and combustion mechanisms, various models that can predict the ignition criteria or flammability limits of hydrogen mixtures have been proposed [11–15]. Le Chatelier proposed a formula to predict the ignition criteria and LFL of gaseous mixtures through an experimental study [11]. The Calculated adiabatic flame temperature (CAFT) model, which cannot consider the heat loss mechanism, has been developed to evaluate the flammability limits of gaseous mixtures for severe accident analysis [12]. Based on this model, a calculated non-adiabatic flame temperature (CNAFT) model was recently developed to improve accuracy by considering the heat loss mechanism [13]. The prediction of this model is more consistent with the experimental results. Kim et al. conducted a numerical study on the LFL of H_2/CO mixture gas according to the initial temperature and concentration using the CNAFT model [15].

Developed flammability models have been applied in lumped parameter (LP) safety analysis codes, such as MAAP and MELCOR, to evaluate the combustion risk of hydrogen in a NPP. MAAP adapts Hertzberg's model and Coward's model to predict the ignition and propagation, respectively [16,17]. In contrast, Le Chatelier's formula was applied to MELCOR as a model for predicting the ignition and flame propagation of hydrogen mixtures [11]. Because of the characteristics of the LP code, the averaged values of a specific compartment can be calculated such that this analysis is mainly conducted to evaluate the maximum hydrogen concentration in a local compartment in the containment [2,18–24]. For the gas mixture in the containment, the possibility of ignition and flame propagation assuming ignition by a source such as a spark was analyzed. Lee et al. analyzed the possibility of ignition in an in-containment refueling water storage tank (IRWST) under station blackout (SBO) and loss of feed water (LOFW) scenario in an advanced power reactor 1400 (APR1400) using the MAAP code [18]. Ahn et al. estimated the generation of both hydrogen and carbon monoxide in OPR1000 under short-term SBO sequences using MELCOR and MAAP codes [2]. For accurate estimation, Kim et al. carried out a detailed modeling that divides the containment compartment into smaller and larger numbers using the MELCOR code [22]. To mitigate the combustion risk during SA, studies have been conducted to evaluate passive facilities and the effectiveness of the mitigating system [25–29]. Saghafi et al. evaluated the

optimal numbers and locations of passive automatic recombiners (PARs) to prevent combustion from occurring under a LOCA in a PWR containment [25]. Furthermore, Lee et al. evaluated the effectiveness of the spray system under a small break loss of coolant accident (SBLOCA), SBO, and total loss of feed water (TLOFW) scenario using the MELCOR code [29].

Previous studies on the plant scale have only focused on combustibility in the containment. Therefore, the combustibility in other systems where the hydrogen concentration is sufficient to be ignited, such as the reactor core, was not considered. Theoretically, it is known that ignition does not occur in the reactor core because there is no oxygen despite the higher hydrogen concentration. However, in a loss of coolant accident (LOCA) scenario, the ignition condition can be satisfied. LOCA generally refers to a circumstance in which a break occurs at the cold leg such that a large amount of coolant in the primary system is discharged into the containment. Accordingly, the pressure of the RCS decreases rapidly. This break region can be a pathway for the inflow of oxygen into the reactor core, which causes hydrogen to be ignited. This flow can be caused by a pressure gradient. The pressure of the containment becomes higher than the pressure of the RCS because various gases are generated by the MCCI during the ex-vessel phase. If there is a generated flame inside the reactor core, the flame has the potential to propagate to the containment when the flame propagation criteria are satisfied. Because this can pose a serious threat to the containment, it is necessary to assess the possibility of its occurrence.

The objective of this study is to investigate the ignition in the reactor core and subsequent propagation mechanisms under the LOCA scenario in OPR1000 using the MELCOR 2.1 code. In addition, the effectiveness of the spray system was evaluated because the changes in the pressure and concentration of flammable gases can affect the overall behavior of ignition and propagation. The detailed objectives of this study are described as follows. The first is to evaluate the possibility of both the existence of oxygen in the reactor core owing to the pressure gradient and resultant ignition. The second is to analyze the propagation mechanism of the generated flame throughout the containment. Because the propagation criterion differs depending on both composition of the gas mixture and direction, the manner in which the flame propagates was analyzed in detail. If it is confirmed that the flame can be propagated to the containment, the third is to analyze the propagation time according to the operating time of the spray system.

2. Methodology

2.1. MELCOR nodalization

To evaluate the local hydrogen concentration of a certain compartment, the containment should be subdivided in detail according to the complicated geometry of the containment structures. Fig. 1 shows the control volumes (CVs) in the MELCOR nodalization for the containment of OPR1000. This modeling is based on methodology of MAAP-CONTAIN analysis and containment nodalization in the final safety analysis report (FSAR) of Shin-Kori NPP which focused on the main compartments for hydrogen release [30]. For Shin-Kori Units 1 and 2, a total of 21 units of PARs are installed in locations such as the annulus and dome regions where it is determined that local hydrogen concentrations can be concentrated. PAR removes hydrogen via chemical reaction with oxygen, as shown in Eq. (1). Because the PAR is a passive system operated without an external power supply, it plays an important role in removing hydrogen in any severe accident situation. To reflect this, therefore, the MELCOR input was also modeled such that PARs exist in the dome and annulus regions based on FSAR through the PAR package. In MELCOR code, PAR package cannot simulate the recombination reaction of carbon monoxide inside the installed PAR. Therefore, it is necessary to model the removal rate of carbon monoxide based on the user's engineering judgement. We assumed that the removal rate of carbon monoxide is 41.7% of that of hydrogen [31], and carbon monoxide is removed since the start of PAR by the hydrogen concentration (2%). In addition, Fig. 2 shows the reactor coolant system (RCS) nodalization of the MELCOR input.

$$2H_2 + O_2 \rightarrow 2H_2O + 1.2*10^8\ (J/kg) \quad (1)$$

2.2. Steady-state calculation

To ensure the reliability of the analysis results, it was necessary to verify the established MELCOR input data. The MELCOR input was verified by comparing and verifying the design parameters related to normal operation situations with the result of the FSAR for Shin-Kori Units 1 and 2. The core thermal power, core inlet/outlet temperature, system pressure and primary/secondary system flow rate were selected as the parameters to be compared. Table 1 shows the calculated results of the selected parameters of MELCOR, and the operation conditions described in the FSAR [30]. Compared to the FSAR values, the MELCOR calculation yielded reasonable results.

2.3. Accident progress sequence

A large break loss of coolant accident (LBLOCA) scenario in which cold leg (CV380) is broken with a size of 9.5 inches was set as the initiating event, and it was assumed that no mitigation strategy was implemented in the base case. The MELCOR calculation was performed until 72 h after the cold leg break. The major sequence of accident progression is summarized in Table 2. Owing to the large break area, a large amount of coolant is discharged to the containment, such that the reactor trip occurs immediately after the accident starts. The core begins to be exposed to steam at 1.62 s. At 124.2 s, the steam temperature in the core exit region reaches 923 K and the accident enters a severe accident situation. Subsequently, the oxidation reaction of cladding occurs, which accelerates the progression of the accident. Eventually, at 258 s, the entire area of the reactor core is exposed to steam, and the cladding begins to melt at 2,200 K at 673 s. Eventually, the RPV fails at approximately 46 min, such that the corium in the lower head is ejected to the reactor cavity. Accordingly, MCCI is initiated immediately after RPV failure, as shown in Fig. 3.

2.4. Ignition and propagation criteria in MELCOR

Ignition can be initiated in a control volume if the concentration of flammable gas satisfies the criteria. In MELCOR, Le Chatelier's formula was applied to determine the ignition threshold [32,33]. The hydrogen concentration must be higher than the criterion, as shown in Eq. (2), where X_{H_2} is the mole fraction of hydrogen. $L_{H_2,ign}$ is the mole fraction limit of hydrogen. While $L_{H_2,ign}$ is 0.07 for the reactor core in which decay heat is being generated, $L_{H_2,ign}$ is 0.1 for the containment with no ignitor and decay heat generation. Additionally, Eq. (3) shows the minimum mole fraction of oxygen required for the ignition of hydrogen, which is 0.05. Finally, the amount of steam should be below the inert level, as shown in Eq. (4), which shows the ignition and inert criteria. If all criteria in Eq. (2) − (4) satisfied, a burn is initiated.

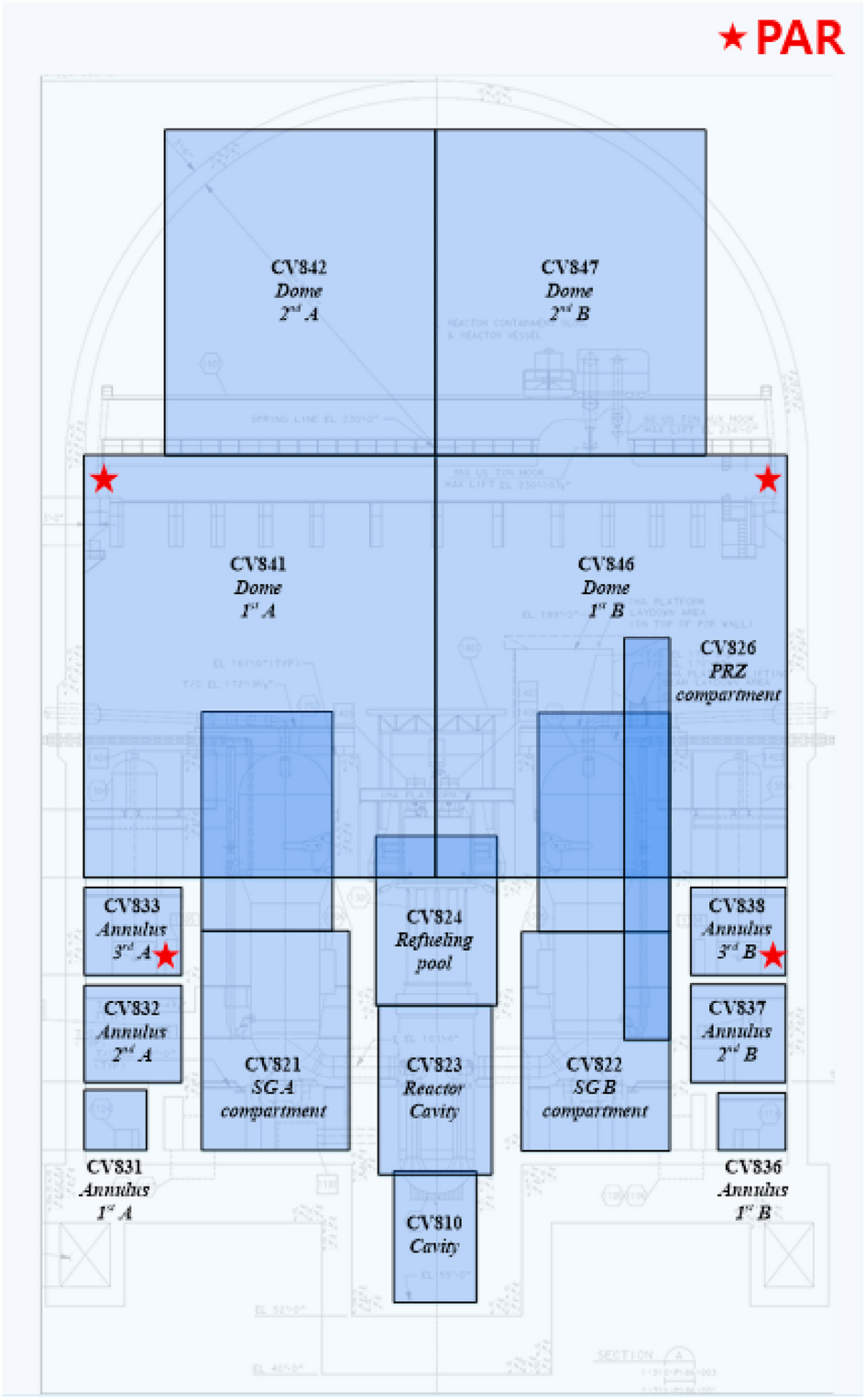

Fig. 1. Nodalization of MELCOR input for containment of OPR1000.

$$X_{H_2} \geq L_{H_2,ign} \quad (2)$$

$$X_{O_2} \geq 0.05 \quad (3)$$

$$X_{H_2O} < 0.55 \quad (4)$$

The generated flame can be propagated if the concentration of flammable gases in the connected control volume satisfies the propagation criteria. For propagation criteria, MELCOR also adapts Le Chatelier's formula that LFL depends on the concentration of hydrogen and carbon monoxide which are flammable gases, and the direction of flame propagation as shown in Table 3 [32,33].

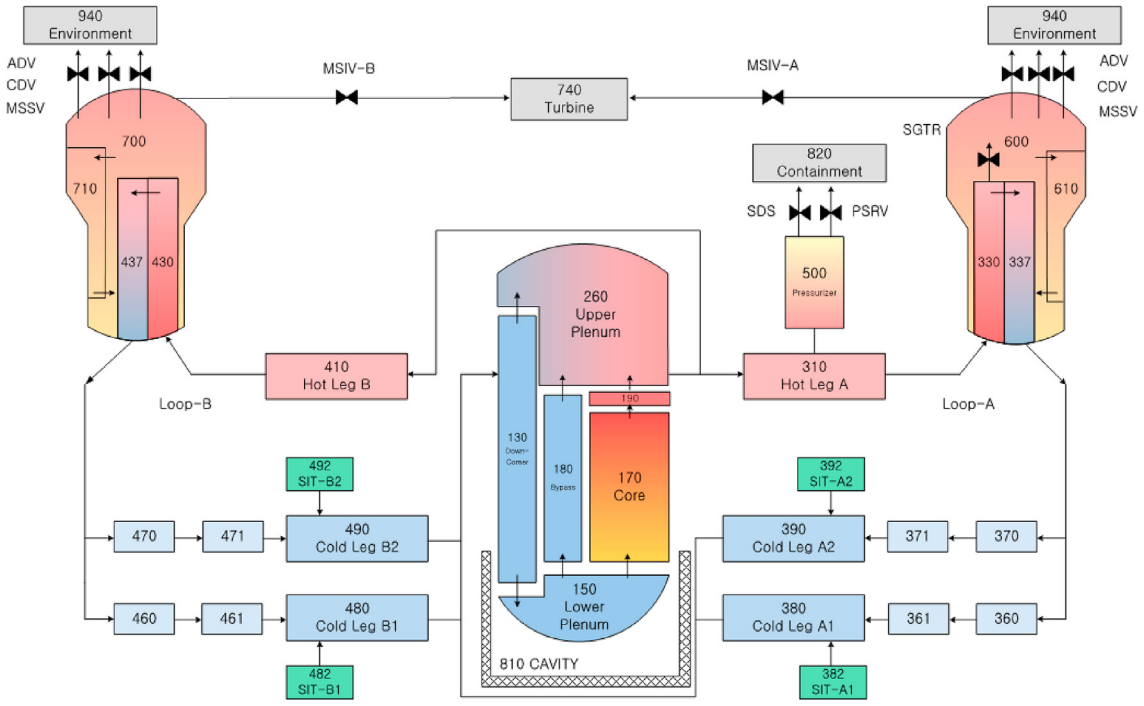

Fig. 2. Nodalization of MELCOR input for RCS of OPR1000.

Table 1
Comparison of design parameters between MELCOR calculation and FSAR [30].

Parameter	FSAR	MELCOR calculation	Error [%]
Core thermal power [MWt]	2,815	2,815	0.0
Core inlet temperature [K]	569	573	0.7
Core outlet temperature [K]	600	603	0.5
RCS pressure [MPa]	15.5	15.5	0.0
SG pressure [MPa]	7.37	7.37	0.0
Primary flow rate [kg/s]	15,306	15,498	1.25
Steam flow per SG [kg/s]	800.0	808.5	1.06

Table 2
Major accident progress sequence under LBLOCA scenario.

Accident progress	Time [s]
Accident start (LBLOCA)	0
Reactor trip	1.5839E-03
RCP trip	1.5839E-03
Core uncovery start	1.62
Entry of SA (CET: 923K)	124.2
Cladding oxidation start	162.5
Core dryout	258
Cladding melt start	673
RPV Failure	2,752.2

Therefore, as shown in Eq. (5) where X_{CO} is the mole fraction of carbon monoxide, the presence of carbon monoxide lowers the required hydrogen concentration for flame propagation in all directions.

$$X_{H_2} + \frac{LFL_{H_2}}{LFL_{CO}} X_{CO} > LFL_{H_2} \tag{5}$$

MCCI is a major accident phenomenon and must be considered for combustion risk assessment because the composition of the gas mixture in the containment during the ex-vessel phase is greatly influenced by the MCCI. First, a large amount of steam is generated

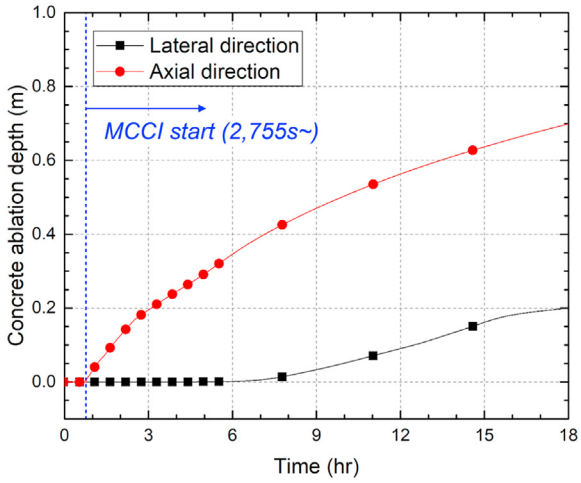

Fig. 3. Reactor cavity concrete ablation depth for axial and lateral direction during MCCI.

because the collected coolant in the reactor cavity is vaporized owing to the high heat transfer from the corium. Second, a large amount of hydrogen and carbon monoxide is generated as the cavity concrete decomposes [34,35]. In particular, for the basaltic concrete of OPR1000, a large amount of carbon monoxide generation can create conditions that are likely to meet criteria for ignition and propagation of the generated flame.

3. Human action time for containment spray system

For OPR1000, when the core exit temperature (CET) exceeds 923 K, it is considered a severe accident. In this situation, mitigation strategies are sequentially executed based on the severe accident management guide (SAMG) as shown in Fig. 4. After the entry of a

Table 3
Propagation criteria in MELCOR [30,31].

Type of gas	Direction of propagation	Lower flammability limit (LFL) [mole fraction]
Hydrogen (H_2)	Upward propagation	0.041
	Horizontal propagation	0.06
	Downward propagation	0.09
Carbon monoxide (CO)	Upward propagation	0.125
	Horizontal propagation	0.138
	Downward propagation	0.15

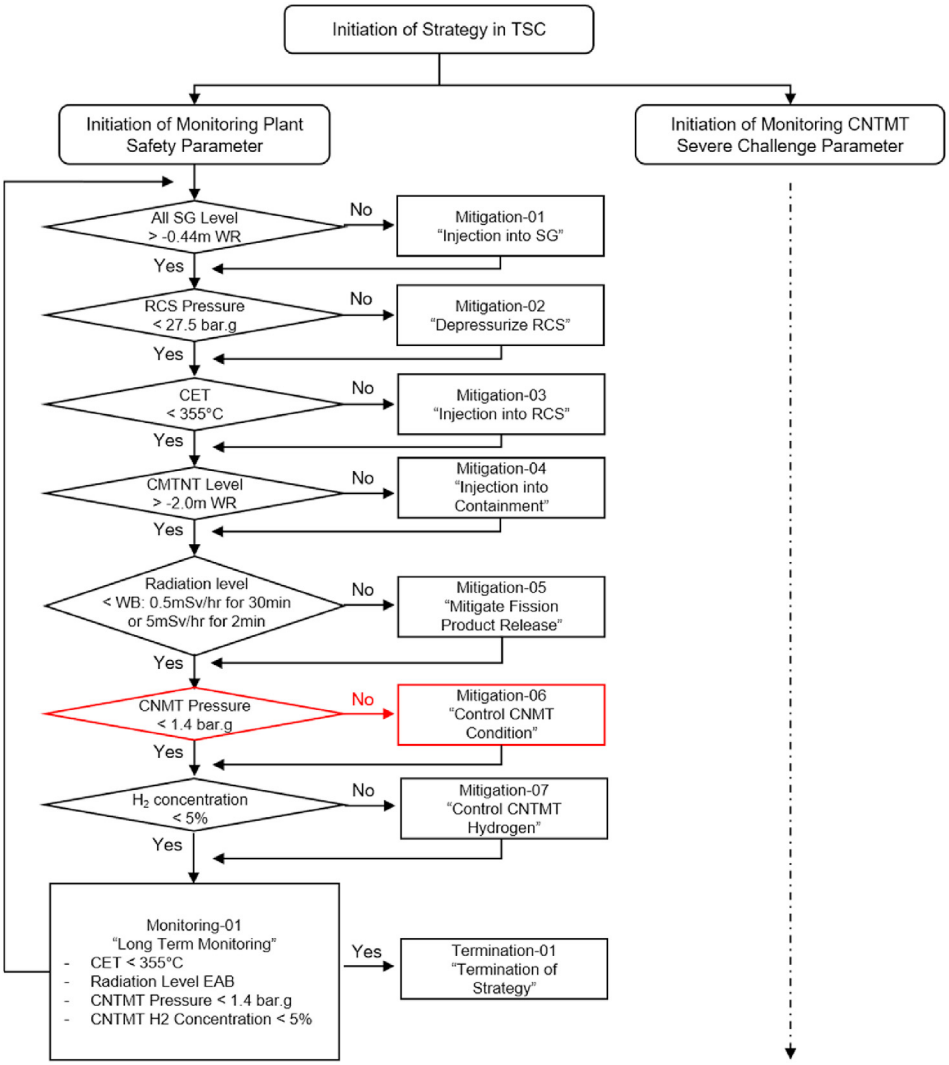

Fig. 4. Severe accident mitigation guide of OPR1000 during sever accident [30].

severe accident, the technical support center (TSC) should be organized and mitigation strategies in the SAMG are performed based on the diagnosis results of the measurement parameters. This process is carried out as long as severe challenge parameters, such as the pressure of containment and hydrogen concentration, do not exceed the set value.

The spray system is an active heat removal system in the containment, which is included in the mitigation strategy-06, as shown in Fig. 4. Mitigation strategy-06 corresponds to containment state control, which is executed when the pressure of the containment rises. Containment spray, fan cooler, and purge systems are available for this stage. In particular, the spray system can depressurize to nearly atmospheric pressure if a heat exchanger is available without the release of radioactive material. In addition, it removes iodine and other radioactive materials from the atmosphere. Therefore, it is considered to be a representative containment depressurization system. In this study, it was assumed that only the spray system is available, while the fan cooler and purge systems are assumed inoperable. Spray system can be activated to control the pressure by operator, based on containment high-pressure signal generated when the pressure exceeds 20.1 psig, corresponding to an absolute pressure of 0.24 MPa [30].

To implement the mitigation strategy, the response time of the operator must be considered. Operator tasks for mitigation

strategies can be classified as monitoring, control, and evaluation [36–38]. Monitoring tasks include checking measurement variables and availability of engineering safety features (ESF), for example, the steam generator water level, safety injection pump, and safety depressurization valve. Adjusting the reactivity, RCS inventory and pressure of RCS, and temperature and pressure of the containment are included in the control task. The evaluation analyzes the possible positive and negative effects according to the execution of the mitigation strategy. Based on research on human action time considering these three tasks, it was assumed that monitoring, control, and evaluation took 30 s, 40 s, and 120 s, respectively [39]. In this case, the required maximum and minimum number of tasks and the required time for execution of each mitigation strategy can be calculated, as shown in Table 4. In particular, the spray system required a maximum of 1.79 h. For a conservative evaluation, in this study, it was assumed that more time than the calculated value is required for operation.

4. Analysis results

4.1. In-core ignition and flame propagation

Fig. 5 shows pressure of containment according to accident progress. As MCCI continues after RPV failure, the pressure gradually increases due to the generated gases such as hydrogen, steam, carbon monoxide, and carbon dioxide. In addition, a pressure rise occurs due to the steam generated by evaporation of the coolant in the reactor cavity. However, at 13.98 h since the accident starts, the pressure rises rapidly up to approximately 0.59 MPa, which exceeds the design pressure of containment. This pressure peak is a phenomenon that appears owing to the effect of flame generated by hydrogen combustion. However, the mole fraction of hydrogen in the containment does not exceed 3%, as shown in Fig. 6. For hydrogen to be ignited, the mole fraction of hydrogen should be at least 10%, as shown in Eq. (2). In other words, ignition cannot occur in the containment. Therefore, it can be predicted that hydrogen is ignited in another specific compartment and the generated flame propagates to the containment. In addition, Fig. 7 shows the generation of carbon monoxide and hydrogen by MCCI. It can be predicted that the flame propagation phenomenon was affected by the existence of carbon monoxide, as shown in Eq. (5).

Fig. 8 compares the pressure of the containment and RCS, both of which are gradually increasing. In particular, the pressure of the RCS tends to be unstable as pressure peaks occur periodically. Based on this tendency, it can be predicted that ignition occurs inside the RCS. At 0.8 h, the pressure of the containment becomes higher than the pressure of the RCS because concrete decomposition gases and steam are generated in the containment while MCCI continues. This pressure gradient between the two systems can form a flow through which the gas flows into the RCS as shown in Fig. 9. Fig. 10 shows that the gas flow from CNMT to RCS occurs via cold leg break

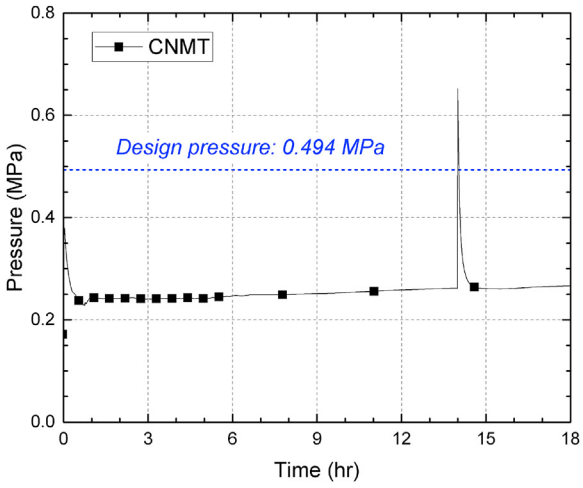

Fig. 5. Pressure of dome region in containment.

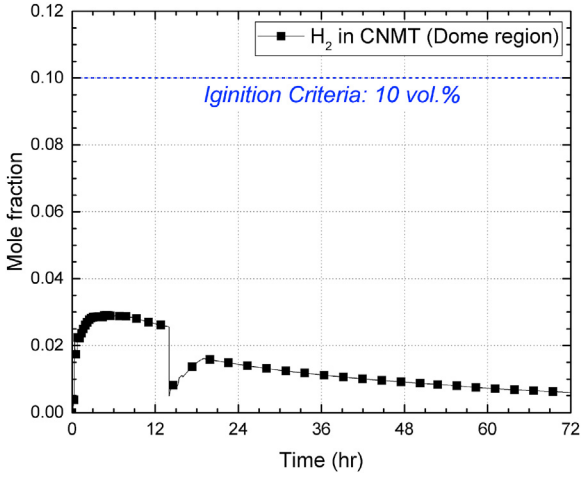

Fig. 6. Mole fraction of hydrogen of dome region in containment.

(negative value of mass flow rate). On the other hand, for a break of RPV, discharge flow occurs because of the heat generation by the initial core degradation in the lower plenum and it is maintained until the pressure equilibrium at 35.2 h. However, there is no core degradation after 1.9 h as shown in Fig. 11. It implies there is no more heat generation so that the pressure gradient is maintained. Therefore, there is a tendency for oxygen to continuously flow into the cold leg break. As the pressure gradient decreases, the mass flow rate also gradually decreases.

Fig. 12 shows the mole fraction of hydrogen and oxygen in the

Table 4
Calculation result of required maximum/minimum number of tasks and time required for each mitigation strategy in SAMG [38].

	Minimum number of tasks			Maximum number of tasks			Time required for execution [hr]	
	Monitoring	Control	Evaluation	Monitoring	Control	Evaluation	Minimum	Maximum
MS-01	56	6	9	91	29	11	0.83	1.45
MS-02	42	3	3	59	24	8	0.48	1.03
MS-03	65	1	6	96	32	8	0.75	1.42
MS-04	28	12	15	36	22	17	0.87	1.11
MS-05	60	39	25	118	70	38	1.77	3.03
MS-06	76	30	21	79	30	24	1.67	1.79
MS-07	27	11	11	110	31	27	0.71	2.16

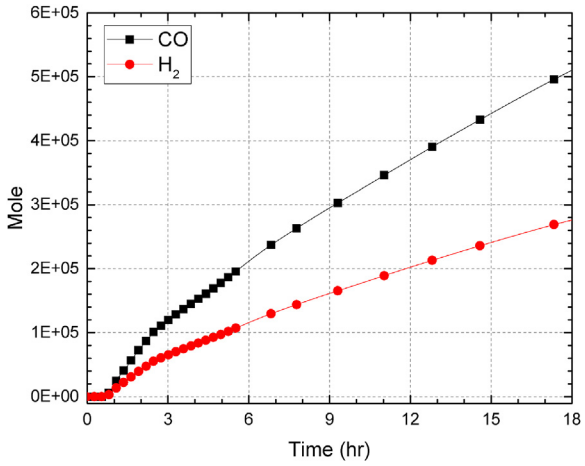

Fig. 7. Hydrogen and carbon monoxide generation by decomposition of concrete during MCCI.

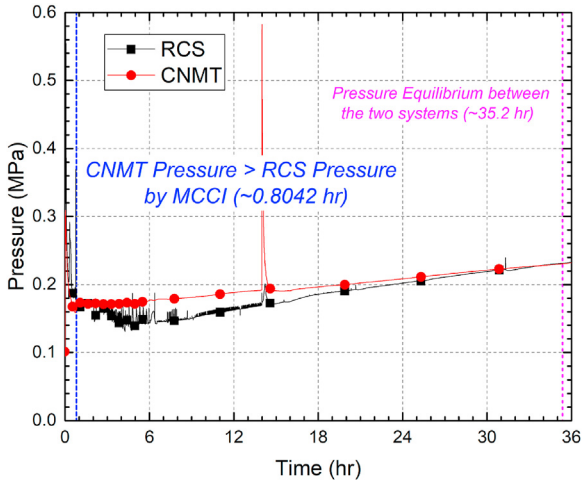

Fig. 8. Comparison of pressure of RCS and containment.

core region. As a large amount of hydrogen is generated owing to the oxidation reaction of cladding, there is a very high concentration of hydrogen. The mole fraction of oxygen increases according to the

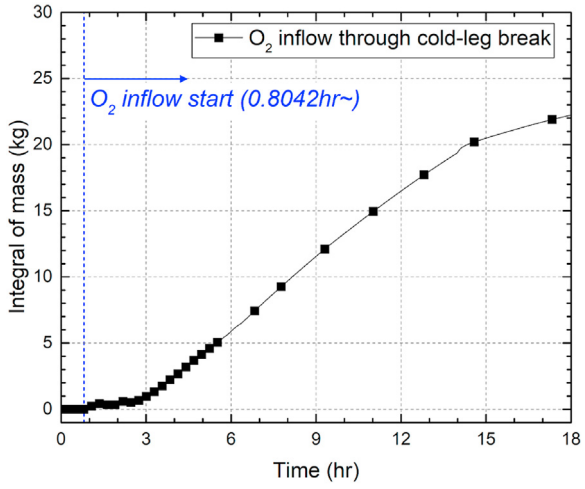

Fig. 9. Integral mass of oxygen inflow into core region through cold leg break.

oxygen inflow into the cold leg and becomes temporarily extinct. Simultaneously, the hydrogen concentration also decreases rapidly. This is because oxygen and hydrogen are consumed when ignition occurs if the oxygen concentration reaches the value required for ignition. Therefore, this process is repeated owing to the continuous inflow of oxygen, which satisfies the oxygen concentration required for ignition (5%). Particularly pressure peak is greatly influenced by the mass of consumed flammable gases for ignition. In addition, the energy generated with hydrogen ignition in the reactor core was propagated into the surrounding space as the pressure wave propagated. This heat transfer mechanism occurred faster than the heat transfer to the surrounding heat structure. It implies that this phenomenon could be a dominant mechanism for reducing the pressure. Fig. 13 shows the pressure and temperature of heat structure, which are related to the heat transfer mechanisms mentioned above. The pressure in the connected space such as upper plenum and core exit region tends to rise rapidly as the pressure wave propagates. The energy propagated along the hot-leg reaches the steam generator U-tube, and the temperature of inner wall of U-tube gradually rises. Therefore, the energy generated inside the reactor core is released so that the pressure is reduced. It occurs very frequently in the early phase of accidents, and the ignition period gradually increases since at 10 h as accidents continue. In addition, as the inflow rate of oxygen also gradually decreases owing to a lower pressure gradient, this tendency increases. Therefore, the amount of oxygen introduced has a large influence on the ignition period. In conclusion, it is confirmed that there is a possibility of occurrence of ignition inside the reactor core.

This flame generated inside the core cannot propagate to the containment until propagation conditions are met at 13.98 h as shown in Fig. 5. For the flame to propagate, the hydrogen concentration should be higher than 4.1% according to Le Chatelier's formula. However, even at the point of the pressure peak in the containment, the mole fraction of hydrogen in the containment is less than 3% as shown in Fig. 6. Therefore, the flame propagates to the containment under the influence of the presence of other combustible gases, such as carbon monoxide. Fig. 14 shows the mole fractions of hydrogen and carbon monoxide in the containment and reactor cavity. Especially, proportion of carbon monoxide tends to rise rapidly. It is because a large amount of carbon monoxide is generated as the reactor cavity concrete are decomposed compared to hydrogen as shown in Fig. 7. This tendency becomes outstanding because the amount removed through PAR is relatively small compared to hydrogen as shown in Fig. 15. In particular, the local concentration in the reactor cavity where flammable gas is being generated tends to be relatively high compared to the containment. At 13.98 h, the concentrations of hydrogen and carbon monoxide in the reactor cavity reach at 8.6% and 3.9%, respectively, which satisfies the LFL for downward propagation criteria. As a result, the flame inside the reactor core propagates to the reactor cavity. Simultaneously, the mole fractions of hydrogen and carbon monoxide in the other compartments in the containment reach 2.56% and 8.65%, respectively. Therefore, the LFL for both the horizontal and upward directions is satisfied owing to the influence of carbon monoxide, allowing the flame in the reactor cavity to propagate to the entire region in the containment. In conclusion, when the LFL is satisfied, the flame generated inside the core propagates to the containment through the reactor cavity and significantly increases the pressure. In this process, the flammable gases in the containment are consumed by the propagated flame, such that the concentration of hydrogen is suddenly lowered at 13.98 h as shown in Fig. 6. Because the mass of the flammable gas in the containment is very large, the pressure exceeds the design pressure. Accordingly, the integrity of the containment is not guaranteed.

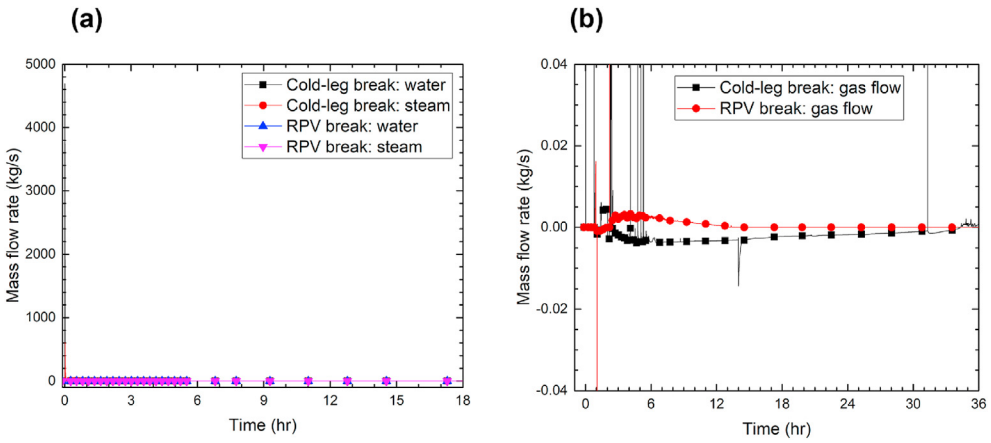

Fig. 10. Mass flow rate of (a) water and steam and (b) gas flow at cold leg and RPV break region.

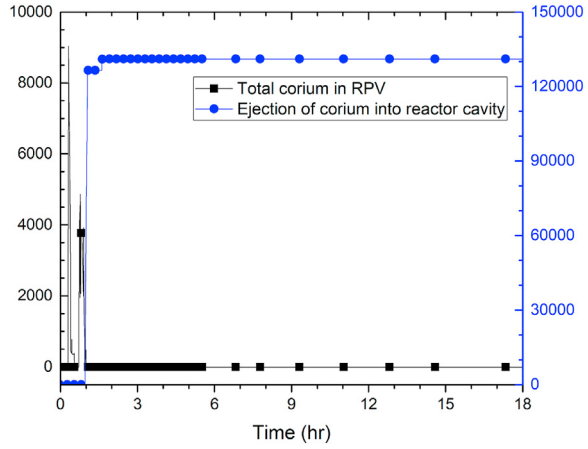

Fig. 11. Mass of (a) total corium in the RPV and (b) corium ejected into the reactor cavity.

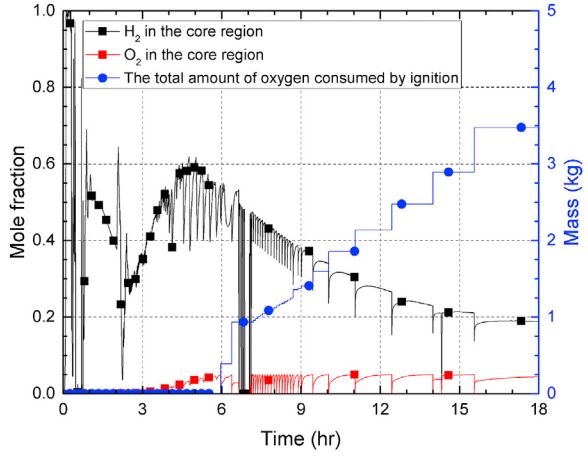

Fig. 12. Mole fraction of hydrogen and oxygen and total amount of oxygen consumed by ignition in core region.

4.2. Comparison with in-containment ignition

It is necessary to compare the flame propagation due to ignition in the reactor core with that caused by ignition in the containment. Ignition in the containment is a very difficult phenomenon to occur in OPR1000 due to installed PAR. Therefore, to compare the tendency between in-core ignition and in-containment ignition (no PAR case), the LBLOCA scenario, in which the PAR is not installed in the containment, was calculated. Other modeling was the same with the in-core ignition case.

For no PAR case, ignition occurs in the reactor cavity after RPV failure because of the higher concentrations of hydrogen and carbon monoxide. At 10.1 h, concentrations of hydrogen and carbon monoxide reached 4.3% and 5.1%, respectively, which satisfies Eq. (6), where L_{H_2} is 0.07 and L_{CO} *is* 0.129. The generated flame near the reactor cavity propagates throughout the whole containment building as shown in Fig. 16. Pressure peak reached approximately 0.68 MPa, which is higher compared to in-core ignition case. With the absence of PAR, the mass of flammable gases in the containment is relatively higher. Therefore, a higher pressure peak occurs as more flammable gases are consumed for the flame to propagate. Even though these phenomena occur after RPV failure in both cases, these have a major effect on the accident consequences because the pressure peaks can threaten the integrity of the containment building posing the leakage of radioactive materials.

$$X_{H_2} + \frac{L_{H_2}}{L_{CO}} X_{CO} > L_{H_2} \tag{6}$$

4.3. Effectiveness of containment spray system

As shown in Fig. 5, in the LBLOCA scenario analyzed in this study, the pressure exceeds 0.24 MPa at 0.89 h, which generates a containment high-pressure signal. When the spray system starts to operate, there are two major considerations for hydrogen risk in this study. First, it should be considered that the flame propagation condition can be satisfied faster because the concentrations of hydrogen and carbon monoxide increase, allowing flames to propagate quickly the containment. Second, the inflow into the RCS changes as the pressure gradient between the RCS and containment decreases. As the inflow of oxygen decreases, the frequency of combustion inside the core decreases. These effects can be greatly affected by the operating time of the spray system because it can vary depending on the gas composition of each of the two systems.

Based on this, a sensitivity analysis was performed to analyze the tendency of the flame propagation according to the operating time of the spray system. The MELCOR simulation matrix is presented in Table 5. When considering the human action time for the maximum number of tasks for mitigation strategy-06, the spray

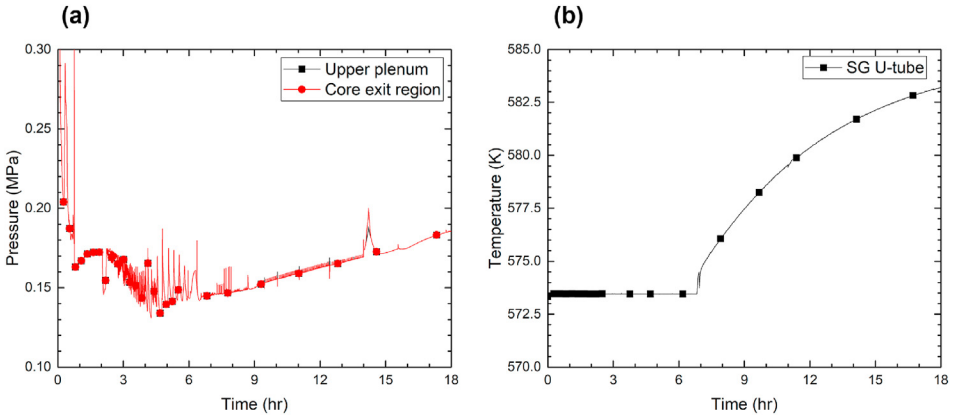

Fig. 13. (a) The pressure in the upper plenum and core exit region and (b) the wall temperature of steam generator U-tube.

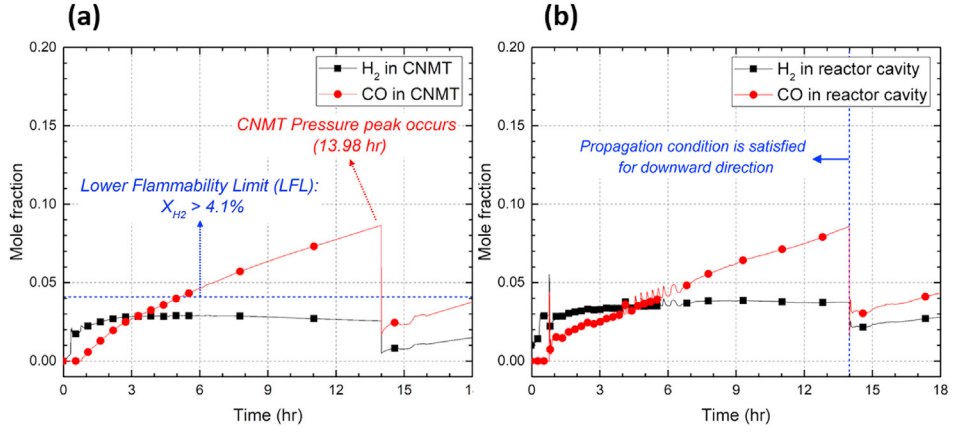

Fig. 14. Mole fraction of hydrogen and carbon monoxide in (a) containment and (b) reactor cavity.

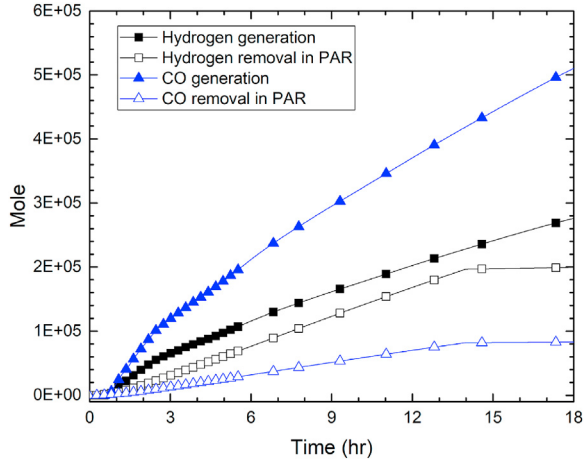

Fig. 15. Generation by MCCI and removal in PAR of hydrogen and carbon monoxide.

system can be operated from a time point of 2.68 h. For a conservative evaluation, in this study, it was assumed that the spray system operates from at least 3 h after the accident, which is at about 2.97 h after entry of SA. Fig. 17 shows the pressure of the containment according to the operating time of the spray system. In the cases where the spray operates before the 7 h point, the flame propagates quickly to the containment, whereas it is delayed in other cases. To confirm the mechanism of these phenomena, cases 1 and 5 are selected as representative analysis cases.

For case 1, Fig. 18 shows that the pressure of the containment decreased immediately to approximately 0.14 MPa after the spray was activated and did not increase thereafter. Therefore, a lower pressure gradient between the RCS and containment was formed compared to the base case. This caused a smaller amount of gas to be introduced into the RCS through the cold leg. Fig. 19 shows the integral mass of the oxygen inflow for case 1. The inflow mass was approximately 12 kg until 18 h, which was approximately 44% of that of the base case. Therefore, the amount of oxygen inflow is significantly affected by the pressure drop caused by the spray system. It can reduce the ignition frequency in the reactor core, as shown in Fig. 20. However, in the early phase of an accident, the hydrogen concentration and inflow rate of oxygen are still high, and ignition occurs frequently. In contrast, the concentration of flammable gas in the containment and reactor cavity increases faster owing to the condensation of steam, as shown in Fig. 21. At 7.58 h, the concentration of flammable gases in the containment already satisfies the propagation criteria for the both the upper and horizontal directions. In other words, if the flame propagates into the reactor cavity region, the condition for propagation throughout the entire containment area is already satisfied. After 11.3 h, the concentration of flammable gases in the reactor cavity reaches the downward propagation condition, as shown in Fig. 21. Accordingly, the flame propagates to the reactor cavity, resulting in a pressure peak as the flame propagates sequentially to the entire region in the

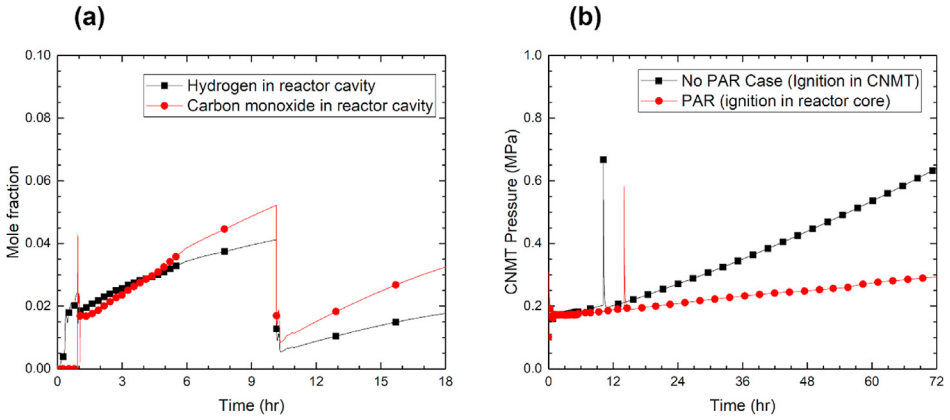

Fig. 16. (a) Concentrations of hydrogen and carbon monoxide in reactor cavity for no PAR case and (b) comparison of containment pressure with and without PAR in containment.

Table 5
MELCOR simulation matrix for sensitivity analysis on operating time of spray system.

Case	Spray start [hr]
Base	–
Case 1	3.0
Case 2	4.0
Case 3	5.0
Case 4	6.0
Case 5	7.0
Case 6	8.0
Case 7	9.0
Case 8	10.0

containment. In other words, even though the frequency of ignition decreases, the containment becomes rather vulnerable in terms of flame propagation owing to the spray system because ignition continues to occur. In conclusion, this results in faster flame propagation to the containment.

In case 5, there is no significant difference in the oxygen inflow rate during the early phase of the accident until the spray starts to operate at 7 h, as shown in Fig. 22. As a result, ignition occurs very actively inside the reactor core during the phase; therefore, the mass of hydrogen consumed by ignition is larger than that in case 1. The inflow rate decreases as the pressure gradient gradually decreases until the spray operation. In addition, as the pressure drops sharply owing to the spray, the flow rate decreases. Therefore, oxygen is less rapidly supplied to the reactor core and the period of ignition tends to become longer at 7.2 h, as shown in Fig. 23. Compared to case 1, the frequency is relatively small. Fig. 24 shows

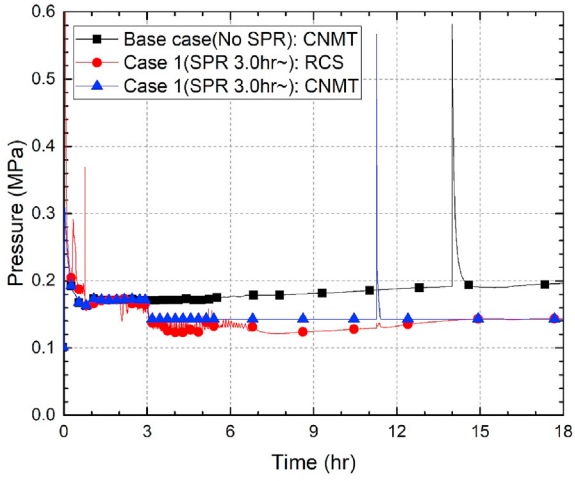

Fig. 18. Pressure of RCS and containment (Case 1).

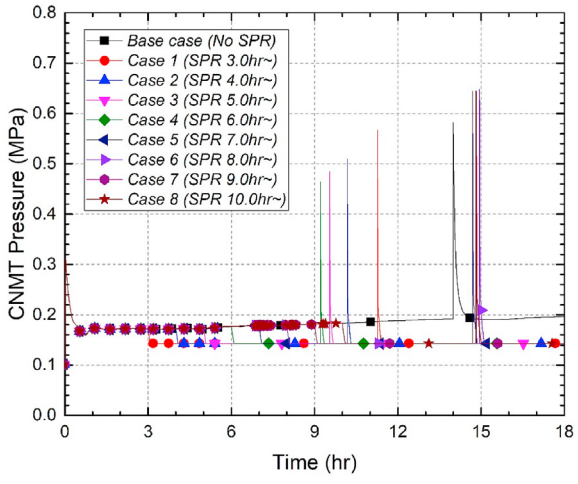

Fig. 17. Pressure of containment according to operating time of spray system.

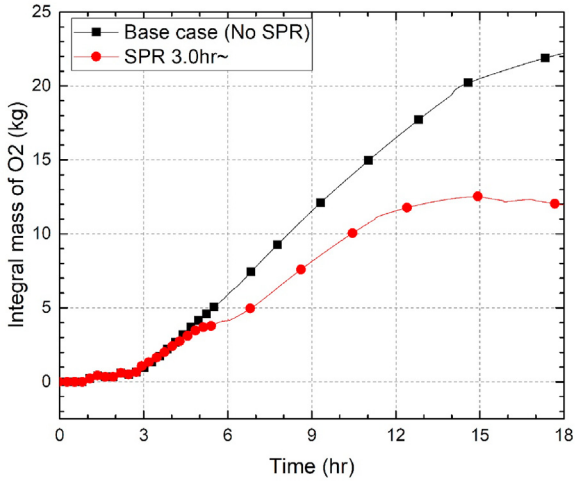

Fig. 19. Integral mass of oxygen inflow into core region through cold leg break (Case 1).

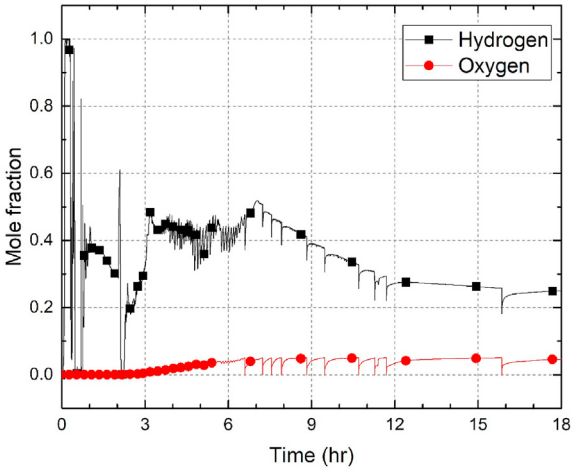

Fig. 20. Mole fraction of hydrogen and oxygen in core region (Case 1).

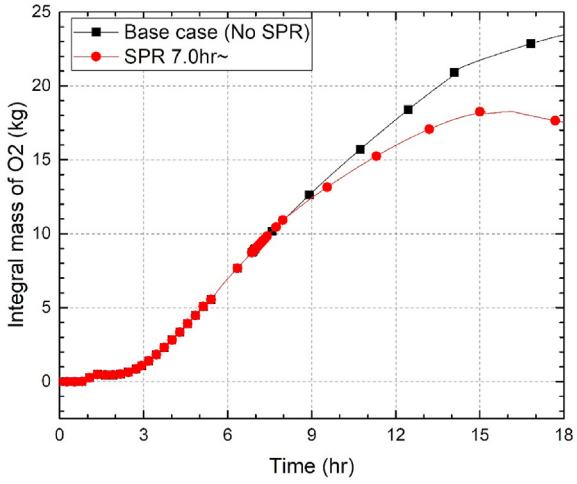

Fig. 22. Integral mass of oxygen inflow into core region through cold leg break (Case 5).

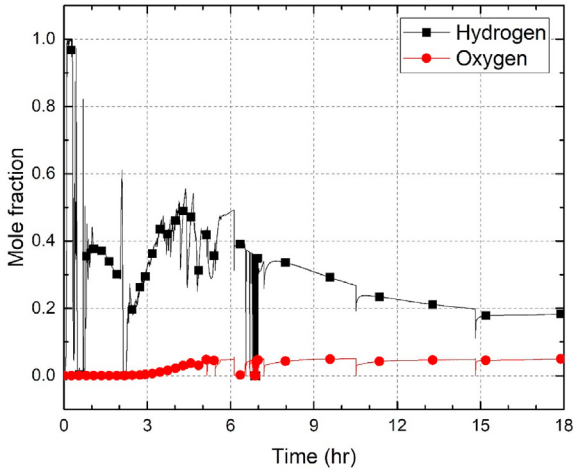

Fig. 23. Mole fraction of hydrogen and oxygen in core region (Case 5).

the concentrations of flammable gases in the containment and reactor cavity. At 7.3 h, the flame propagation criteria for both the upward and horizontal directions are already satisfied. In addition, at 11.8 h, the condition for the flame to be propagated to the reactor cavity is already reached. However, the flame propagation occurs at 14.8 h according to the pressure peak, which occurs later than the base case. The cause of this trend is the ignition frequency in the reactor core. After the early phase of the accident, from 7.2 h, the ignition frequency exceeds 3 h as the oxygen supply decreases. Therefore, even though conditions have been reached for the flame to propagate, the pressure peak does not occur until ignition occurs at 14.8 h. In other words, in this case, it is possible to delay flame propagation. In conclusion, based on the sensitivity analysis of the operating time of the spray system, an excessive operation can have negative effects, hence it is necessary to discuss and analyze the appropriate operation time.

5. Summary and conclusions

In this study, we investigated the mechanism by which the flame generated inside the reactor core propagated to the containment. In the LOCA scenario, after RPV failure, the pressure of the containment increased continuously owing to the gases generated during the MCCI. The pressure difference by these gas generations between the RCS and containment can cause an inflow of gases through the cold leg break, which means that oxygen can exist inside the reactor core. Then, because the hydrogen concentration inside the reactor core is very high, ignition can occur. This generated flame can propagate to the containment when the

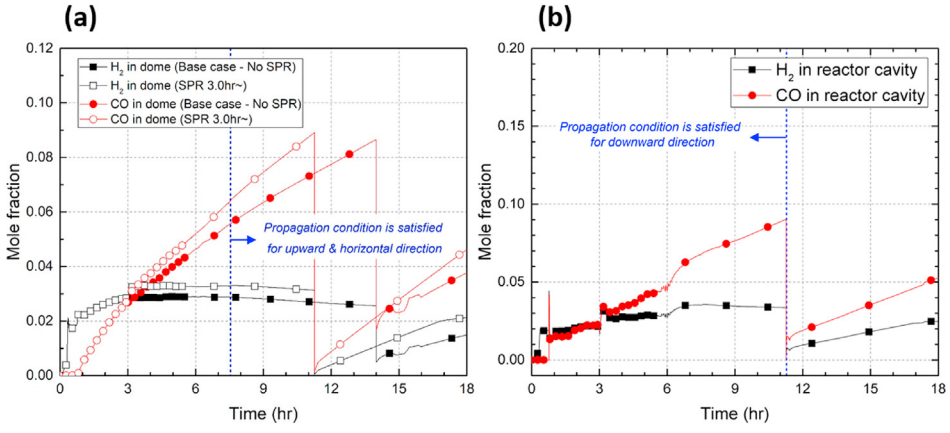

Fig. 21. Mole fraction of hydrogen and carbon monoxide in (a) containment and (b) reactor cavity (Case 1).

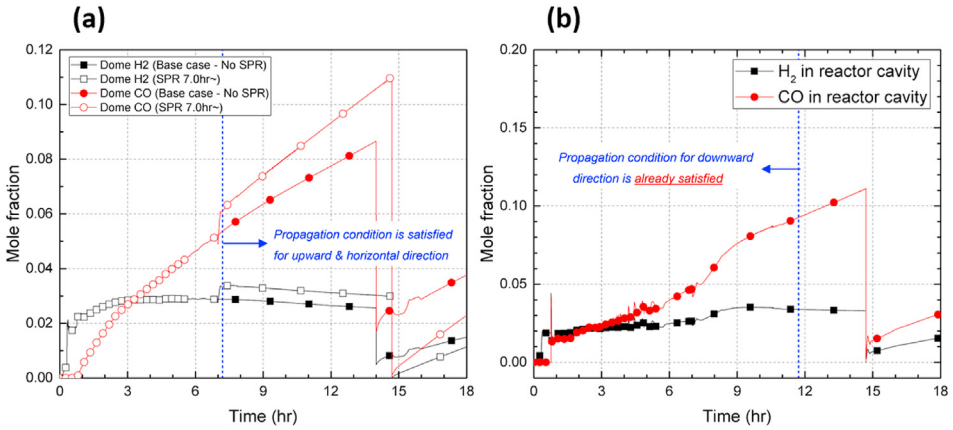

Fig. 24. Mole fraction of hydrogen and carbon monoxide in (a) containment and (b) reactor cavity (Case 5).

concentration of flammable gas in the containment satisfies the flame propagation criteria. Based on this background, the mechanisms of ignition and flame propagation in OPR1000 using the MELCOR 2.1 code were analyzed.

In addition, the effectiveness of the spray system operation based on the value of the measurement parameters in the SAMG during a severe accident was also analyzed. This is because the time at which the flame propagates to the containment depends on the change in the pressure gradient and the concentration of flammable gases. Based on the number of tasks for the mitigation strategy, human action time was considered. The major findings and future work are as follows:

(1) The possibility of ignition inside the reactor core under LBLOCA was confirmed. After RPV failure, gas generation during MCCI led to a higher pressure of containment compared to RCS. This pressure gradient caused an inflow of oxygen through the cold leg break. Accordingly, ignition frequently occurred inside the reactor core. As the pressure difference gradually decreased, the inflow rate of oxygen decreased, and thus, the ignition period became longer. In particular, in-core ignition could not be possible under the MBLOCA scenario, in which the size of the cold leg break is 3.5 inch, in our preliminary analysis. It is because the pressure equilibrium between the two connected systems was quickly formed in the initial accident phase because no more core degradation occurs after RPV failure. Therefore, there is no oxygen inflow through cold leg break and RPV break. In conclusion, it was judged that in-core ignition could be possible when the accident proceeds very quickly by larger cold leg break area that the pressure equilibrium is delayed due to core degradation after the RPV failure. Analyzing the minimum cold leg break area for making the in-core ignition will be the important topic of our future work.

(2) When the concentration of flammable gases in the reactor cavity area satisfied the flame propagation criteria, the generated flame in the reactor core propagated to the reactor cavity area. Even though the concentration of hydrogen in the dome region in the containment was lower than 3%, it immediately propagated to the entire containment area because the presence of a high concentration of carbon monoxide satisfied the propagation criteria for both the horizontal and upward directions. These phenomena caused the pressure of containment to rise rapidly, exceeding the design pressure of the NPP, such that the integrity of the NPP was not guaranteed. Therefore, flammable gases generated by MCCI are very important for combustion risk assessment. In addition, the concentration of flammagle gases in the containment was greatly affected by the PAR performance because carbon monoxide is also removed by the recombination reaction. Therefore, removal rate is a very important factor, which implies that it is necessary to conduct a detailed analysis on the carbon monoxide recombianation by the PARs.

(3) The early operation of the spray system led to faster flame propagation. In the early phase of the accident, despite the decrease in the oxygen inflow rate, ignition still occurred actively because the hydrogen concentration was very high. At this phase, the increase in the concentration of flammable gases in the containment was rather vulnerable to propagation. As the accident progressed to the late phase, repeated ignition and a lower pressure gradient led to a decrease in the hydrogen concentration and oxygen inflow rate, respectively. In this phase, if the oxygen inflow decreased, the ignition frequency decreased rapidly. In other words, although the propagation criteria were already satisfied, the flame propagated later owing to delayed ignition. Therefore, it is necessary to consider the flame propagation conditions before operating the spray system under the LBLOCA.

(4) In this study, we attempted to propose the possibility of an accident progress that was not reported previously. These phenomena could be due to the characteristics of lumped code or to a real phenomenon because the effect of the geometry of the structure and the detailed combustion mechanism cannot be considered owing to the characteristics of the lumped code. For example, the inflow rate of oxygen may vary depending on the direction of the cold leg break. In addition, the flame propagating from the core to the cavity can be obstructed by the coolant in the cavity. Therefore, it is necessary to conduct additional precise analysis on the practicality of these phenomena under accident conditions through CFD code. This analysis will be the focus of our future work.

(5) In Republic of Korea, accident management plan should include an evaluation of the ability to mitigate the severe accidents. Accordingly, it should be evaluated the exposure dose of residents near the NPP site. In terms of effective dose, the possibility of in-ignition and subsequent flame propagation are very significant factors because the corresponding pressure peak which exceeds the design pressure poses

leakage of radioactive materials. Therefore, it is judged that this is an important phenomenon, and should be analyzed in detail.

Declaration of competing interest

The authors declare that they have no known competing financial interests or personal relationships that could have appeared to influence the work reported in this paper.

Acknowledgements

This work was supported by the Nuclear Safety Research Program through the Korea Foundation of Nuclear Safety (KoFONS) using the financial resource granted by the Nuclear Safety and Security Commission (NSSC) of the Republic of Korea (grant number 2003006-0120-CG100). Additionally, this work was supported by the National Research Foundation of Korea (NRF) and funded by the Ministry of Science, ICT, and Future Planning, Republic of Korea (grant number NRF-2021M2D2A2076382).

References

[1] B.R. Sehgal, Nuclear safety in light water reactors: severe accident phenomenology, Ch. 3 Early Containment (2012).
[2] K. Il Ahn, S.Y. Park, W. Choi, S.J. Kim, Best-practice severe accident analysis for the OPR1000 short-term SBO sequence using MELCOR2.2 and MAAP5, Ann. Nucl. Energy 160 (2021), https://doi.org/10.1016/j.anucene.2021.108350.
[3] A. Keçebaş, M. Kayfeci, Hydrogen properties, Solar Hydrogen Prod.: Process. Syst. Technol. (2019) 3–29, https://doi.org/10.1016/B978-0-12-814853-2.00001-1.
[4] Z.M. Shapiro, T.R. Moffette, Hydrogen Flammability Data and Application to PWR Loss-Of-Coolant Accident, 1957. Wapd-Sc-545.
[5] J.E. Hustad, O.K. Sønju, Experimental studies of lower flammability limits of gases and mixtures of gases at elevated temperatures, Combust. Flame 71 (3) (1988) 283–294, https://doi.org/10.1016/0010-2180(88)90064-8.
[6] F. Van den Schoor, F. Verplaetsen, The upper flammability limit of methane/hydrogen/air mixtures at elevated pressures and temperatures, Int. J. Hydrogen Energy 32 (13) (2007) 2548–2552, https://doi.org/10.1016/j.ijhydene.2006.10.053.
[7] C. Appel, J. Mantzaras, R. Schaeren, R. Bombach, B. Kaeppeli, A. Inauen, An experimental and numerical investigation of turbulent catalytically stabilized channel flow combustion of hydrogen/air mixtures over platinum, Proc. Combust. Inst. 29 (1) (2002) 1031–1038, https://doi.org/10.1016/S1540-7489(02)80130-4.
[8] M. Ilbas, A.P. Crayford, I. Yilmaz, P.J. Bowen, N. Syred, Laminar-burning velocities of hydrogen-air and hydrogen-methane-air mixtures: an experimental study, Int. J. Hydrogen Energy 31 (12) (2006) 1768–1779, https://doi.org/10.1016/j.ijhydene.2005.12.007.
[9] S. Gupta, E. Schmidt, B. Von Laufenberg, M. Freitag, G. Poss, F. Funke, G. Weber, Thai test facility for experimental research on hydrogen and fission product behaviour in light water reactor containments, Nucl. Eng. Des. 294 (October) (2015) 183–201, https://doi.org/10.1016/j.nucengdes.2015.09.013.
[10] P. Wang, Y. Zhao, Y. Chen, L. Bao, S. Meng, S. Sun, Study on the lower flammability limit of H2/CO in O2/H2O environment, Int. J. Hydrogen Energy 42 (16) (2017) 11926–11936, https://doi.org/10.1016/j.ijhydene.2017.02.143.
[11] H. Le Chatelier, Estimation of firedamp by flammability limits, Ann. Mines 19 (1891) 388–395.
[12] M. Vidal, W. Wong, W.J. Rogers, M.S. Mannan, Evaluation of lower flammability limits of fuel-air-diluent mixtures using calculated adiabatic flame temperatures, J. Hazard Mater. 130 (1–2 SPEC. ISS.) (2006) 21–27, https://doi.org/10.1016/j.jhazmat.2005.07.080.
[13] J. Jeon, W. Choi, S.J. Kim, A flammability limit model for hydrogen-air-diluent mixtures based on heat transfer characteristics in flame propagation, Nucl. Eng. Technol. 51 (7) (2019) 1749–1757, https://doi.org/10.1016/j.net.2019.05.005.
[14] M. Vidal, W. Wong, W.J. Rogers, M.S. Mannan, Evaluation of lower flammability limits of fuel-air-diluent mixtures using calculated adiabatic flame temperatures, J. Hazard Mater. 130 (1–2 SPEC. ISS.) (2006) 21–27, https://doi.org/10.1016/j.jhazmat.2005.07.080.
[15] S. Kondo, K. Takizawa, A. Takahashi, K. Tokuhashi, A. Sekiya, A study on flammability limits of fuel mixtures, J. Hazard Mater. 155 (3) (2008) 440–448, https://doi.org/10.1016/j.jhazmat.2007.11.085.
[16] Y.S. Kim, J. Jeon, C.H. Song, S.J. Kim, Improved prediction model for H2/CO combustion risk using a calculated non-adiabatic flame temperature model, Nucl. Eng. Technol. 52 (12) (2020) 2836–2846, https://doi.org/10.1016/j.net.2020.07.040.
[17] M. Hertzberg, Flammability limits and pressure development, in: M. Berman (Ed.), H2-air Mixtures (NUREG/CR–2017-Vol3), 1981. United States.
[18] H.F. Coward, G.W. Jones, Limits of Flammability of Gases and Vapors, 1952.
[19] B.C. Lee, et al., An optimal hydrogen control analysis for the in-containment refueling storage tank (IRWST) of the Korean next generation reactor (KNGR) containment under severe accidents, Int. Conf. Nuclear Eng. Nice France (2001).
[20] OECD/NEA, Flame Acceleration and Deflagration-To-Detonation Transition in Nuclear Safety, 2000. NEA/CSNI/R(2000)7.
[21] OECD/NEA, ISP-49 on Hydrogen Combustion, 2011. NEA/CSNI/R(2011)9.
[22] OECD/NEA, Status Report on Hydrogen Management and Related Computer Codes, 2014. NEA/CSNI/R(2014)8.
[23] N.K. Kim, J. Jeon, W. Choi, S.J. Kim, Systematic hydrogen risk analysis of OPR1000 containment before RPV failure under station blackout scenario, Ann. Nucl. Energy 116 (2018) 429–438, https://doi.org/10.1016/j.anucene.2018.02.050.
[24] J. Wang, Y. Zhang, K. Mao, Y. Huang, W. Tian, G. Su, S. Qiu, MELCOR simulation of core thermal response during a station blackout initiated severe accident in China pressurized reactor (CPR1000), Prog. Nucl. Energy 81 (2015) 6–15, https://doi.org/10.1016/j.pnucene.2014.12.008.
[25] G. Huang, L. Fang, Analysis of hydrogen control in severe accidents of CANDU6, Ann. Nucl. Energy 60 (2013) 301–307, https://doi.org/10.1016/j.anucene.2013.04.019.
[26] M. Saghafi, F. Yousefpour, K. Karimi, S.M. Hoseyni, Determination of PAR configuration for PWR containment design: a hydrogen mitigation strategy, Int. J. Hydrogen Energy 42 (10) (2017) 7104–7119, https://doi.org/10.1016/j.ijhydene.2017.01.110.
[27] J. Deng, X.W. Cao, A study on evaluating a passive autocatalytic recombiner PAR-system in the PWR large-dry containment, Nucl. Eng. Des. 238 (10) (2008) 2554–2560, https://doi.org/10.1016/j.nucengdes.2008.04.011.
[28] S. Şahin, M.S. Sarwar, Hydrogen hazard and mitigation analysis in PWR containment, Ann. Nucl. Energy 58 (2013) 132–140, https://doi.org/10.1016/j.anucene.2013.03.001.
[29] E. Lopez-Alonso, D. Papini, G. Jimenez, Hydrogen distribution and Passive Autocatalytic Recombiner (PAR) mitigation in a PWR-KWU containment type, Ann. Nucl. Energy 109 (2017) 600–611, https://doi.org/10.1016/j.anucene.2017.05.064.
[30] KHNP (Korea Hydro & Nuclear Power Co.), Shin Kori 1&2 Final Safety Analysis Report, 2008.
[31] C. Kim, H. Kim, I. Ryu, Y. Moon, Comparison MAAP5.03 with MAAP5.04 from Recombination of CO point of view, in: Transactions of the Korean Nuclear Society Autumn Meeting, 2016.
[32] L.L. Humphries, R.K. Cole, D.L. Louie, V.G. Figueroa, M.F. Y, MELCOR Reference Manual, 2015.
[33] L.L. Humphries, R.K. Cole, D.L. Louie, V.G. Figueroa, M.F. Y, MELCOR Users Guide, 2015.
[34] M.T. Farmer, S. Lomperski, R.W. Aeschlimann, D.J. Kilsdonk, N.E. Division, OECD/MCCI-2010-TR02 OECD MCCI Project Category 2 Coolability Engineering Enhancement Tests: Final Report, 2010.
[35] M.T. Farmer, S. Lomperski, D.J. Kilsdonk, R.W. Aeschlimann, N.E. Division, OECD/MCCI-2010-TR07 OECD MCCI-2 Project Final Report, 2010.
[36] ANS (American Nuclear Society), Time Response Design Criteria for Safety-related Operator Actions, ANSI/ANS-58.8-1994, 1994. La Grange Park, Illinois.
[37] W. Jung, J. Park, J. Kim, J. Ha, Analysis of an operators' performance time and its application to a human reliability analysis in nuclear power plants, IEEE Trans. Nucl. Sci. 54 (5) (2007) 1801–1811, https://doi.org/10.1109/TNS.2007.905163.
[38] J. Park, Y. Kim, J.H. Kim, W. Jung, S.C. Jang, Estimating the response times of human operators working in the main control room of nuclear power plants based on the context of a seismic event - a case study, Ann. Nucl. Energy 85 (2015) 36–46, https://doi.org/10.1016/j.anucene.2015.03.053.
[39] Y.G. No, C. Lee, S. Hur, P.H. Seong, Development of a method for identifying severe status requiring early entrance of SAMG considering human action time, Ann. Nucl. Energy 122 (2018) 317–327, https://doi.org/10.1016/j.anucene.2018.09.006.